Human parainfluenza virus infection remodels the host cell glycome

Plabon Kumar Das[1], Larissa Dirr[1], Benjamin Bailly[1], Patrice Guillon[1], Arun Everest-Dass[1] and Mark von Itzstein[1].

[1]Institute for Biomedicine and Glycomics, Griffith University, Gold Coast Campus, Queensland 4222, Australia.

Abstract

Human parainfluenza virus type 3 (HPIV-3) remains a major cause of respiratory illness particularly among young children, the elderly and immunocompromised individuals. Despite significant efforts in therapeutic discovery research, there is neither an effective antiviral nor a vaccine available against HPIV-3. Host cell glycosylation is known to play a pivotal role in virus entry and replication. While some host glycan-based cellular receptors for HPIV-3 have been identified, the dynamics of the host-cell glycome upon HPIV-3 infection has never been studied. Herein, we report the first mass spectrometry-based study that provides direct insight into the remodelling of the human lung adenocarcinoma cell (A549) glycome upon HPIV-3 infection. Our results reveal significant remodelling of host-cell glycome, including increased expression of oligomannose and reduced expression of sialylated complex-type *N*-glycans. In addition, we observed altered *O*-glycan expression, with upregulation of core 1 and downregulation of core 2 type structures in infected cells compared to mock-infected controls. HPIV-3 infection also led to distinct remodelling of glycosphingolipid glycans. Together, these findings present the first evidence that HPIV-3 infection alters host-cell glycome, offering new insights into the virus' impact on host-cellular processes.

Keywords: respirovirus, host-cell glycome, mass spectrometry, glycome remodelling.

30 ## Introduction

31 Human parainfluenza viruses (HPIVs) are among the most common causes of
32 respiratory tract infections in children under the age of five, the elderly, and
33 immunocompromised individuals, often resulting in high mortality rates[1]. The most common
34 clinical manifestations reported for HPIV infections include colds, croup, bronchiolitis,
35 bronchitis, and pneumonia. HPIV infections account for 40% of paediatric hospitalizations for
36 lower respiratory tract infection and 75% of croup cases across the world, annually[1]. Despite
37 the significant health burden posed by HPIV infections, neither antiviral drugs nor vaccines are
38 currently available. The infection begins in the nose and oropharynx and then spreads to the
39 lower respiratory tract in severe cases, with ciliated epithelial cells of both the upper and lower
40 respiratory tracts being the primary targets of HPIVs[2,3]. There are four major serotypes of
41 HPIV, designated as serotype 1 to serotype 4. HPIV-3 is the most prevalent HPIV subtype
42 worldwide, including Australia, causing seasonal outbreaks in spring mostly after influenza
43 outbreaks[4]. Regardless of serotypes, cell surface carbohydrates (glycans) play an important role
44 in the life cycle of HPIVs[1]. Glycans, carbohydrate-based biopolymers linked by glycosidic
45 bonds, are present in all living organisms. They play significant roles in biology, including
46 maintaining the cell's physical and structural integrity, contributing to the formation of
47 extracellular matrix, mediating signal transduction, assisting in protein folding, and facilitating
48 infection by pathogens[5]. In particular, glycans play numerous roles in viral pathogenesis,
49 including as host cell receptors for adhesion of the virus particle (e.g. influenza virus)[6],
50 protection of the antigenic epitope of viral glycoproteins from the host immune response (e.g.
51 human immunodeficiency virus)[7], and subversion of the immune response by acting as an
52 antibody decoy (e.g. Lassa virus)[8]. Like influenza viruses, HPIV-3 recognizes sialic acids on
53 the host cell via its haemagglutinin-neuraminidase (HN) protein. The neuraminidase activity
54 of the HN protein enables the virus to remove sialic acid residues from glycoproteins and
55 glycolipids on the host cell surface, thereby aiding the release of new virus particles from the
56 infected host-cell[9]. While the important role of glycans for entry and release of HPIV is known,
57 the dynamics of the host-cell glycome expression upon infection remains to be determined.

58 Recent advancements in chromatography, ionization techniques and mass spectrometry
59 have significantly enhanced our ability to characterize glycans through relatively user-friendly
60 workflows and high-throughput methodologies[10]. Liquid chromatography (LC), employing
61 porous graphitized carbon (PGC) as a stationary phase, coupled with electrospray ionization
62 (ESI) tandem mass spectrometry (PGC-LC-ESI-MS/MS) can separate and detect the structural

63 isomers of glycans based on their retention time and fragmentation pattern[11]. Using the
64 PGC-LC-ESI-MS/MS-based workflow, we aimed to characterize the dynamics of the host-cell
65 glycome—including *N*-, *O*-, and glycosphingolipid (GSL) glycans—during HPIV-3 infection
66 in a human lung epithelial cell model (A549 cells).

67 Based on our findings, our study supports the notion that there is an extensive
68 remodelling of the host-cell glycome upon HPIV-3 infection at the measured timepoints of
69 24 h and 48 h. Notably, a significant increase in oligomannose-type and a concomitant decrease
70 in sialylated complex-type *N*-glycans was observed post-infection. HPIV-3 infection also led
71 to increased expression of core 1 and decreased expression of core 2 type *O*-glycans compared
72 to mock-infected cells. These alterations in *N*-glycan and *O*-glycans were accompanied by a
73 significant modulation of GSL glycans in HPIV-3 infected cell. Our findings demonstrate that
74 HPIV-3 remodels the host-cell glycome, providing a comprehensive characterization of this
75 remodelling event and offering new insights into HPIV-3 pathogenesis.

76 Experimental procedures

77 *Cell culture, virus and infection assays*

78 Human lung adenocarcinoma epithelial cells (A549; ATCC, CCL-185) were
79 maintained in Dulbecco's Modified Eagle Medium (DMEM) (Gibco, Cat. no. 10313021) media
80 supplemented with 5% foetal bovine serum (FBS, Gibco, Cat. no. 10099141), 1%
81 Antibiotic-Antimycotic (100X, Gibco, Cat. no. 15240062), 1% MEM Non-essential Amino
82 Acid (100X, Sigma, Cat. no. M7145), 1% L-Glutamine 200 mM (100X, Gibco, Cat. no.
83 25030081) and incubated at 37 °C in a humidified chamber containing 5% CO_2. Human
84 parainfluenza virus type 3 (HPIV-3 JS), genetically modified to incorporate green fluorescent
85 protein (GFP), was obtained from ViraTree (Product # P323). Virus propagation was performed
86 in Rhesus monkey kidney epithelial (LLC-MK2; ATCC, CCL-7) cells using DMEM media
87 supplemented with 1% Antibiotic-Antimycotic, 1% MEM Non-essential Amino Acid, 1%
88 L-Glutamine ($DMEM_{inf}$) at 35 °C in a humidified chamber containing 5% CO_2. Approximately
89 2 million A549 cells were seeded in a 75 cm^2 flask 48 h prior infection. Cells were washed 2
90 times with phosphate buffer saline (PBS) and 5 times with $DMEM_{inf}$. Cell monolayer was
91 infected with HPIV-3 for 1 h at 35 °C and 5% CO_2, with multiplicity of infection (MOI) of 3
92 in triplicates. The mock-infected control was treated the same way as their infected counterpart
93 except for adding viral inoculum. Both infected and mock-infected cells were incubated for 24
94 h and 48 h at 35 °C in a humidified chamber containing 5% CO_2.

95 *Protein and glycosphingolipid (GSL) extraction*

96 Cell culture media from both infected and mock-infected control were collected and
97 mixed with 5 volumes of ice-cold $(CH_3)_2CO$ (Sigma-Aldrich, Cat no. 650501) before storing
98 at -20 °C overnight to precipitate secreted proteins. Infected and mock-infected cells were first
99 washed four times with PBS to remove any residual media, including viral progeny. The cells
100 were then detached with a scrapper and lysed in 1X cold RIPA lysis buffer (Thermo Fisher,
101 Cat. no. 89900) supplemented with 1X protease inhibitor (Roche, cat. no. 11697498001). The
102 mixture was incubated overnight at 4 °C, followed by sonication for 30 min in an ultrasound
103 sonicator (VEVOR Ultrasonic Cleaner). Proteins and glycosphingolipids from cell lysates were
104 extracted through standard chloroform, methanol, and water extraction method described
105 elsewhere[12]. Briefly, 550 µL of chloroform (Sigma-Aldrich, Cat no. 1.02445) were added to
106 each sample and sonicated for 15 min, followed by addition of 350 µL of methanol (Merck,
107 Cat. no. 1.06035). The cell lysates were incubated at room temperature for 15 min with gentle
108 shaking, followed by centrifugation at 3000 x g for 20 min. Upper phase containing
109 glycosphingolipid were transferred to clean tubes. A mixture of 400 µL of chloroform/methanol
110 (2:1) and 400 µL of methanol/water (1:1) was added to the pellets and vortexed vigorously.
111 The mixture was sonicated again for 15 min followed by centrifugation at 3000 x g for 20 min.
112 Upper phase was collected and added to the previous collected sample. An additional 400 µL
113 methanol/water (1:1) mixture was added to the initial chloroform/methanol (2:1) phase and the
114 separation steps were repeated. Proteins were pelleted, by adding 750 µL methanol to the lower
115 phase, followed by centrifugation at 10000 x g for 20 min. The supernatant containing lipids
116 were combined with previously collected upper aqueous phase and subsequently dried using a
117 speed vac concentrator (Thermo Scientific; Savant SPD131DDA). The protein pellets were
118 air-dried and then resuspended in 100 µL 8 M urea. The secreted protein samples were
119 centrifuged at 5000 x g for 40 min to pellet the proteins. Supernatant was decanted and the
120 protein pellets were resuspended in 100 µL 8 M urea. Bicinchoninic acid (Thermo-Fisher, Cat.
121 no. 23227) assay was performed to quantify the proteins. Proteins were reduced and alkylated
122 by adding dithiothreitol (25 mM final concentration) at 60 °C for 1 h and Iodoacetamide
123 (50 mM final concentration) (Merck, Cat. no. 16125), for 30 min in dark at room temperature.

124 *Release of* N- *and* O-*glycans*

125 The glycomics workflow, including the release, reduction, desalting, and PGC clean-up
126 of *N*-, *O*-, and GSL glycans from protein and lipid samples, was performed according to a

127 previously published protocol[13], unless otherwise stated. Dot blotting of proteins on
128 polyvinylidene fluoride (PVDF) membrane (0.45 μm pore size, Millipore, Cat. no.05317) was
129 performed before the release of *N*-, and *O*-glycans. PVDF membrane was first activated with
130 ethanol (Merck, Cat. no. 459828). Approximately 30 μg of proteins were spotted on the
131 membrane. Protein spots were stained using direct Blue (Sigma-Aldrich, Cat. no. 212407),
132 excised, and transferred to a flat bottom polypropylene 96-well plate (Merck, Cat. no.
133 CLS3364), blocked with 1% (w/v) polyvinylpyrrolidone (Sigma-Aldrich, Cat no. PVP40) in
134 50% (v/v) methanol and washed 3 times with 100 μL ultrapure water (Sigma-Aldrich, Cat no.
135 1.15333). The *N*-glycans were then released using PNGase F (1000 units for each reaction)
136 (New England Biolabs, Cat. no. P0709L) for 16 h at 37 °C. The released *N*-glycans were
137 collected after agitation of the sealed plate on a shaker. The PVDF membrane wells were then
138 washed with 2 × 20 μL of water and collated with previously collected *N*-glycans.
139 Subsequently, 10 μL of 100 mM ammonium acetate (pH 5) was added to the collected
140 *N*-glycans, followed by incubation at room temperature for 1 h. The samples were then dried
141 under vacuum and kept in the freezer until further use.

142 To release the *O*-glycans from the same PVDF membrane spot, 2.5 μL of MeOH was
143 added to each spot to pre-wet them. About 50 μL 0.5 M $NaBH_4$ in 100 mM KOH was added in
144 each well and the plate was sealed with parafilm to prevent evaporation. Then the plate was
145 incubated for 18 h at 50 °C. The reaction was neutralized with 5 μL glacial CH_3COOH.

146 *Purification and enzymatic release of GSL glycans*

147 Purification of GSLs was performed according to a previously described method[14]. In
148 brief, the dried aqueous and lipid-containing phases were resuspended in 100 μL of MeOH for
149 30 min on a shaker, followed by the addition of 100 μL of H_2O. Then, the sample was loaded
150 onto a tC18 RP cartridge (Waters, Cat. no. WAT036820), that was preconditioned with 1 mL
151 of chloroform/MeOH (2:1; v/v), 1 mL of MeOH and 2 mL of MeOH/H_2O (1:1; v/v). After the
152 addition of the sample, the cartridge was washed with 2 mL of MeOH/H_2O and the elution was
153 performed with 2 mL of MeOH and 2 mL of chloroform and MeOH (2:1; v/v). The combined
154 eluate was dried under vacuum and stored at -20 °C until further use. The enzymatic release of
155 the GSL head group was performed by following manufacturer's instructions (New England
156 Biolabs, Cat. no. P0773S). In brief, the dried GSLs were resuspended in 36 μL of H_2O, 4 μL
157 of EGCase I reaction buffer and 2 μL of EGCase I enzyme. The reaction mixture was then
158 incubated at 37 °C for 36 h. The separation and purification of the released glycans from the

159 were performed on tC18 RP cartridge, which was preconditioned with 2 mL of MeOH and 2
160 mL of H_2O. After loading the sample, the cartridge was washed twice with 200 µL of H_2O. The
161 flowthrough containing the released glycans, along with the column washes, was collected and
162 dried under vacuum.

163 *Reduction of* N-*glycans and GSL glycans*

164 The Glycans were reduced by adding 25 µL of 1 M $NaBH_4$ (Sigma-Aldrich, Cat. no.
165 213462) in 100 mM KOH (Sigma-Aldrich, Cat. no. 757551), through incubation at 50 °C for
166 3 h. Three microliters of glacial CH_3COOH (Merck, Cat. no. 5.33001.0050) was added to
167 quench the reaction.

168 *Desalting of reduced glycans*

169 Reduced *N*-, *O*-, and GSL glycans were desalted using cation exchange. The columns
170 were self-packed with 25 µL of strong cation-exchange resin (50W-X8) slurry (BIO-RAD, cat.
171 no. 1421451) in MeOH onto a ZipTip C_{18} resin tip. The columns were preconditioned
172 sequentially with 3 × 50 µL of 1 M HCl (Sigma-Aldrich, cat. no. 320331), 3 × 50 µL of MeOH,
173 and 3 × 50 µL of ultrapure water. The samples were applied to the preconditioned columns,
174 and the original sample tube was rinsed with 50 µL of ultrapure water, which was then added
175 to the column. The glycans were subsequently eluted with 2 × 50 µL aliquots of ultrapure water.
176 The eluted glycans were then dried and treated with 4 × 100 µL of MeOH to remove the borate
177 salt.

178 *PGC clean-up of* N-*,* O- *and* GSL *glycans*

179 Carbon material was removed from the carbograph SPE cartridge (BGB Analytik AG,
180 cat. no. SPU-5122423) and a slurry was prepared with a concentration of 50 mg/mL in
181 methanol. About 25 µL of the slurry was loaded into a ZipTip with 0.6 µL C18 resin. The
182 columns were pre-conditioned with 3 × 50 µL of 0.1% CF_3COOH (Sigma-Aldrich, cat. no.
183 302031) and 3 × 50 µL of 90% CH_3CN (Sigma-Aldrich, cat. no. 1.00029), 0.1% CF_3COOH.
184 The glycan samples were loaded in 50 µL of 0.1% CF_3COOH. Finally, the samples were eluted
185 with 50 µL of 50% CH_3CN, 0.1% CF_3COOH. The eluted glycans were then dried using a speed
186 vac concentrator (Thermo Scientific; Savant SPD131DDA) and stored at -20 °C until further
187 use.

188

189 *PGC-LC-ESI-MS/MS of released* N- *and* O- *and GSL glycans*

190 The PGC-LC-ESI-MS/MS glycomics analysis was performed using an amaZon speed
191 ion trap (IT-MS, Bruker, Bremen, Germany) linked to an Ultimate 3000 UHPLC system
192 (Dionex/Thermo). Five microliters of glycan sample were injected by the autosampler and
193 separated using an analytical PGC column (Hypercarb™ PGC Column, Thermo Fisher
194 Scientific, 3 µm particle size, inner diameter 1 mm x 30 mm, maintained at 45 °C). Ten
195 millimolar NH_4HCO_3 was used as buffer A and 70% Acetonitrile in 10 mM NH_4HCO_3 was
196 used as solvent B in the mobile phase. The flow rate was set at 15 µL/min for *N*-, *O*-, and GSL
197 glycans. The gradient system used to separate the *N*-glycans was as follows: 1% B at 0 min;
198 14% B at 6 min; 25% B at 25 min; 70% B at 45 min; 98% B at 50 min; 1% B at 51 min; 1% B
199 at 65 min. *O*- and GSL glycans were separated using the following gradient: 1% B at 0 min;
200 25% B at 25 min; 70% B at 45 min; 98% B at 47 min; 1% B at 51 min; 1% B at 65 min. Eluted
201 glycans were then ionised using ESI in negative ion mode and detected with an ion-trap mass
202 analyser. A *m/z* range of 460–1,800 was set for data-dependent precursor scanning. The
203 collision induced dissociation (CID) fragmentation was used as the fragmentation method
204 where the five most intense precursors of each MS scan were selected for tandem MS. Capillary
205 voltage was set at 3.3 kV, with nitrogen drying gas flow rate 6 L/min at 8.70 psi nebulizer
206 pressure. An ICC target of 70,000 and maximum accumulation time of 100 ms were used.
207 Smart parameter setting (SPS) was set to 1200 *m/z*.

208 *Glycan structure determination and relative quantitation*

209 The MS data was manually analysed using Compass Data analysis version 4.4 (Bruker
210 Daltonics) and then quantitated with Skyline version 22.2[15]. Monosaccharide compositions
211 were determined using the Glycomod tool available on the Expasy[16] with a mass tolerance of
212 0.5 Da. The glycan structures were assigned manually from the tandem mass spectra and
213 characterized with the GlycoWorkbench version 2.1[17]. The fragmentation spectra were also
214 further matched with UniCarb KB to confirm all the structures[18]. Normalised relative
215 intensities of individual glycan structures were calculated in Microsoft Excel and using
216 GraphPad Prism, and to perform statistical analysis

217 *Statistical analysis*

218 All the experiments were done in triplicates, and statistical analysis was performed in
219 GraphPad Prism (version 9). *P* values were calculated by performing an unpaired two-tailed

220 Welch's *t*-test at 95% confidence level. Data visualization was performed in R Studio, with
221 final figure preparation and refinement done in Adobe Illustrator.

222 *Glycan Representation*

223 Glycan structures were visualized by cartoons generated using GlycoWorkbench
224 Glycans were depicted according to the Consortium for Functional Glycomics (CFG) notation:
225 *N*-acetylglucosamine (*N*; blue square), fucose (F; red triangle), mannose (H; green circle),
226 galactose (H; yellow circle), *N*-acetylneuraminic acid (S; purple diamond), and
227 *N*-glycolylneuraminic acid (Sg; light blue diamond).

228 **Results**

229 *HPIV-3 infection triggers significant changes in* N*-glycan expression in the host cell*

230 We hypothesized that viral infection could alter glycan expression in host cells, which
231 may influence processes such as progeny virion release, cell–cell and cell–matrix interactions,
232 and overall cell signalling. To study the impact of infection on host-cell glycosylation, we
233 analysed *N*-glycan expression of cell-extracted and secreted proteins from both mock-infected
234 and HPIV-3 infected A549 cells, at 24 h and 48 h timepoints post-infection. In total, 70
235 *N*-glycan species (including structural and compositional isomers) were observed across
236 infected and mock-infected cells, varying from 5 to 17 monosaccharides. The glycan species
237 were manually interpreted and validated based on the existence of specific fragment ions in
238 their MS/MS spectra[19]. The identified *N*-glycans were grouped based on structural features
239 (oligomannose, complex sialylated, complex neutral, hybrid, and paucimannose). Relative
240 abundances of each glycan species from infected and mock-infected cells were statistically
241 analysed. The differential expression of *N*-glycans in infected and mock-infected cells is
242 provided in Figure 1a-c.

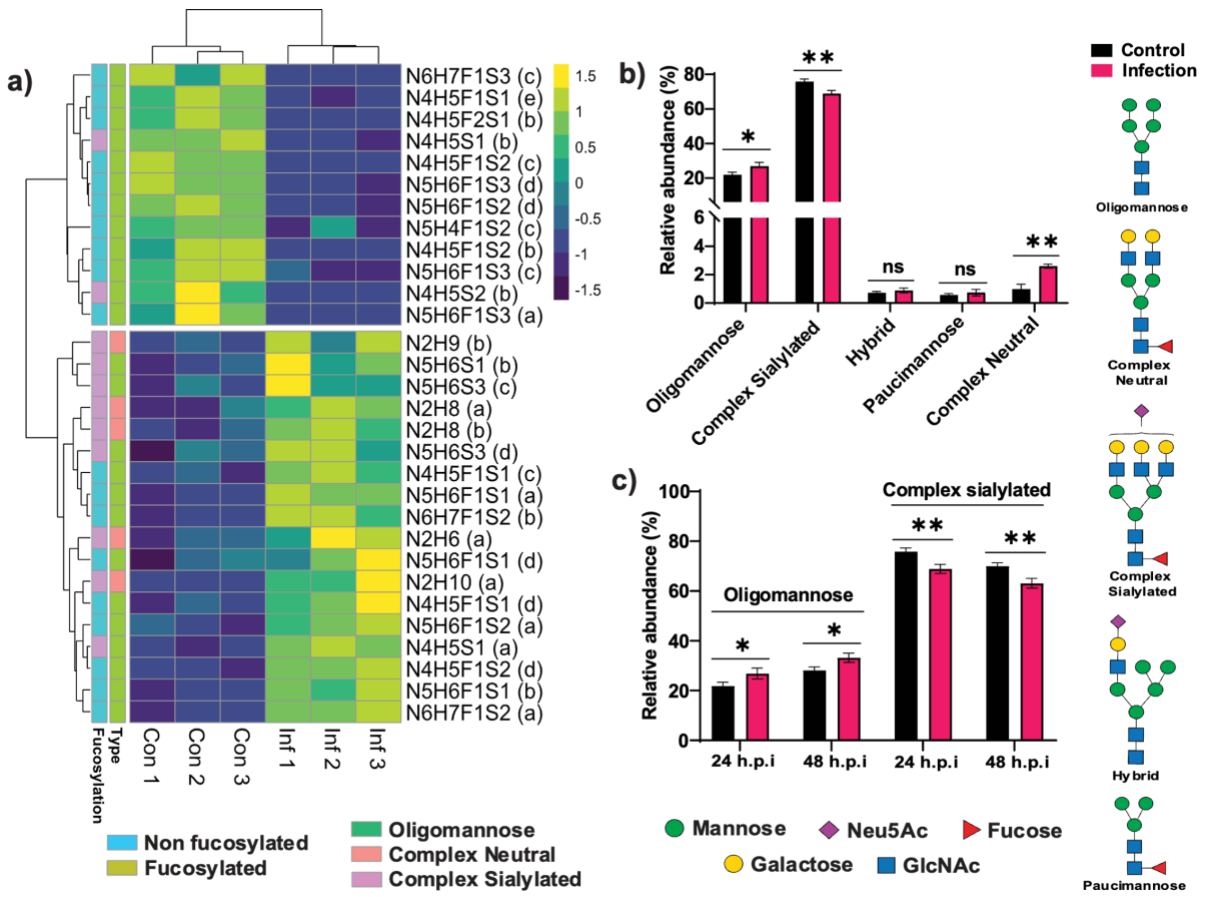

Figure 1: ***HPIV-3 infection modulates expression of* N*-glycans on cell-extracted proteins.*** *a) Heatmap representing the relative abundance of significantly altered* N*-glycans before and 24 h post-infection. b) Differential expression of all major types of* N*-glycans on infected and mock-infected cells at 24 h post-infection. c) Altered expression of oligomannose-type and sialylated complex-type* N*-glycans at 24 h and 48 h timepoints post-infection. n=3, *P<0.05, **P<0.01, ***P<0.001, ns: not significant, unpaired Welch's t-test. N:* N*-Acetyl Hexosamine; H: Hexose; F: Fucose; S:* N*-Acetyl Neuraminic Acid; h.p.i: hours post-infection.*

In the context of total *N*-glycan composition, we observed that sialylated complex-type *N*-glycans and oligomannose-type glycans were the most abundant, comprising more than 90% of total *N*-glycans detected in both mock-infected and HPIV-3 infected A549 cells. We observed a significantly higher expression of oligomannose-type *N*-glycans (from 21.87% ± 1.50% in mock-infected to 26.87% ± 2.18% in infected cells) at 24 h post-infection (Figure 1b). We also observed diverse sialylated structures ranging from mono-sialylated biantennary to tri-sialylated tri-antennary complex glycans. HPIV-3 infection resulted in significant reduction of sialylated complex-type *N*-glycans in infected cells, decreasing from 75.85% ± 1.47% in mock-infected to 68.90% ± 1.81% in infected cells (Figure 1b). To identify if the altered expression of glycans in infected cells is stable, we analysed the glycan expression also at 48 h post-infection. Notably, similar changes in both oligomannose-type and sialylated complex-type *N*-glycans were also observed at 48 h post-infection. For example, an approximately 5% increase in oligomannose-type and a 7% decrease in sialylated

263 complex-type *N*-glycans were detected in infected cells (Figure 1c). Moreover, we saw a subtle,
264 yet statistically significant, increase (~1.5%) in the expression of complex neutral-type
265 *N*-glycans upon 24 h and 48 h post-infection. Two other major glycan types, hybrid and
266 paucimannose, remained unchanged during infection at 24 h and 48 h.

267 Cell secreted proteins play important roles in maintaining cell communication and
268 signalling, and glycans that decorate these secreted proteins are key to these interactions[20].
269 Considering these important roles, we analysed the glycans released from secreted proteins of
270 both infected and mock-infected cells and compared their relative abundances (Figure 2a).

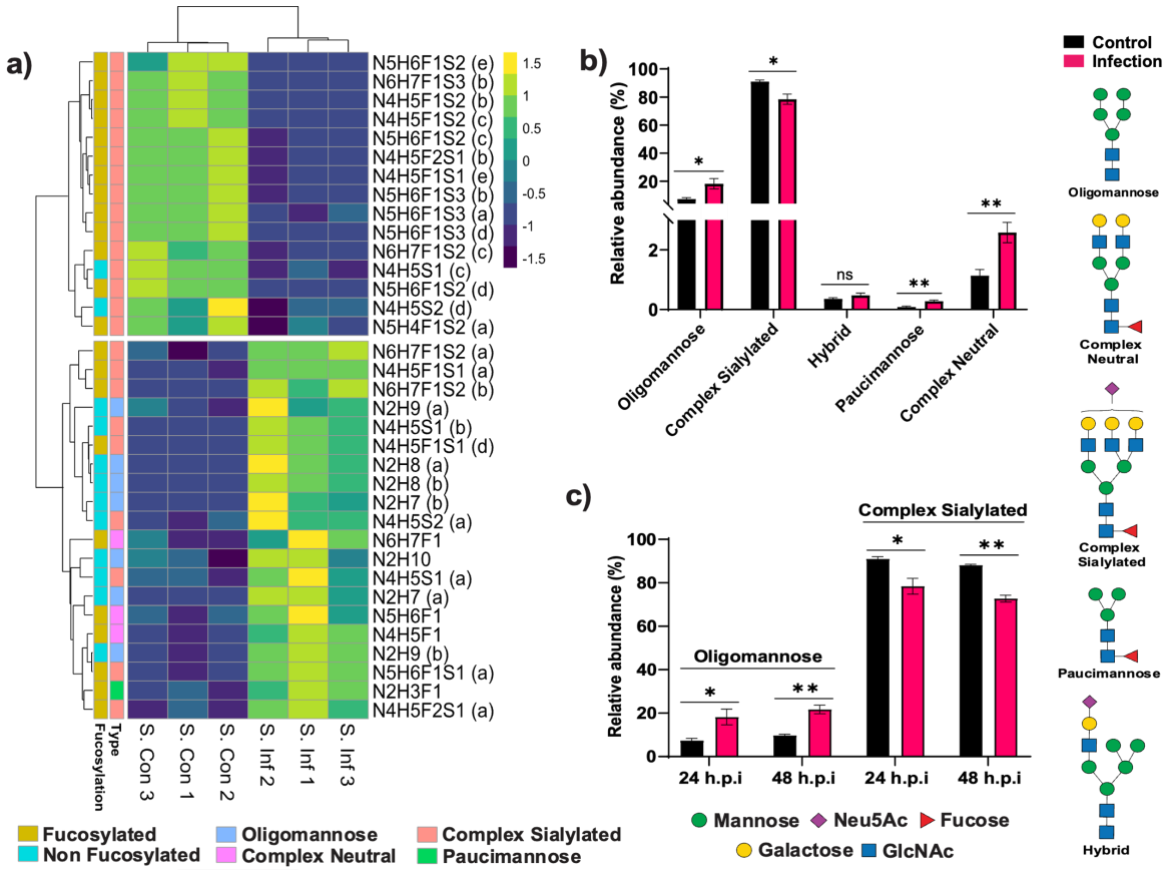

271

272 *Figure 2:* ***HPIV-3 infection modulates expression of* N*-glycans on secreted proteins.*** *a) Heatmap represents the relative*
273 *abundance of significantly altered* N*-glycans before and at 24 h post-infection. b) Differential expression of all major types of*
274 N*-glycans in infected and mock-infected cells at 24 h post-infection. c) Altered expression of oligomannose-type and sialylated*
275 *complex-type* N*-glycans at 24 h and 48 h post-infection. n=3, *P<0.05, **P<0.01, ns: not significant, unpaired Welch's t-test.*
276 *N:* N*-Acetyl Hexosamine; H: Hexose; F: Fucose; S:* N*-Acetyl Neuraminic Acid; h.p.i: hourss post-infection.*

277 The *N*-glycome composition of secreted proteins differed slightly from that of cell-extracted
278 proteins. Approximately 90% of *N*-glycans on secreted proteins were processed from
279 oligomannose to sialylated complex-type structures, whereas cell-extracted proteins contained
280 about 70-74% sialylated complex-type *N*-glycans. However, in agreement with *N*-glycans on
281 cellular proteins, expression of sialylated complex-type glycans was decreased from

282 91% ± 1.08% in mock-infected control to 78.44% ± 3.66% in HPIV-3 infected cells (24 h
283 post-infection). We also observed a significant increase of ~11% in oligomannose-type glycans
284 in response to viral infection (24 h post-infection) (Figure 2b). Notably, these changes were
285 nearly twice as pronounced as those observed in cell-extracted proteins, which showed a 7%
286 decrease in sialylated complex-type and a 5% increase in oligomannose-type *N*-glycans.
287 Likewise, HPIV-3 infection also modulated the *N*-glycome composition of secreted proteins at
288 48 h post-infection. The level of oligomannose-type glycans was augmented by more than 12%,
289 whereas the expression of sialylated complex-type *N*-glycans was reduced by more than 15%
290 on secreted proteins collected from HPIV-3 infected cells compared to mock-infected control
291 (Figure 2c). The complex neutral type comprised of 1% to 2% of the total secreted protein
292 *N*-glycome in mock-infected cells. However, the expression of this glycan type was observed
293 to be doubled at both 24 h and 48 h post-infection (Figure 2b). There were no significant
294 changes observed in relative intensities of hybrid and paucimannose-type *N*-glycans on
295 secreted proteins after infection irrespective of the time points (Figure 2b).

296 *Differential expression of oligomannose and sialylated complex-type* N-*Glycans at the*
297 *individual glycan level*

298 Next, we examined whether changes in oligomannose and sialylated complex-type
299 *N*-glycans followed a similar pattern at the level of individual glycan species. A detailed
300 analysis enabled us to identify that, although overall abundance of oligomannose-type
301 *N*-glycans increased from the mock-infected control (21.87% ± 1.50%) to infected cells
302 (26.87% ± 2.18%), not all oligomannose species exhibited a similar trend. We observed that
303 individual oligomannose species were either increased or remained constant post-infection
304 (Figure S1, S2). Oligomannose glycans containing 5 to 9 mannose units were identified across
305 infected and mock-infected cells. Of these, both isomers of Man 8, one isomer of Man 9, Man
306 6, Man 7 and Man 9 Glc 1 were increased at 24 h post-infection on cell-extracted proteins
307 (Figure S1a). Likewise, each isomer of Man 7 to Man 9 was upregulated, whereas others
308 remained constant after 48 h of infection when compared to the mock-infected control
309 (Figure S2a). This trend was consistent for secreted proteins both at 24 h and 48 h
310 post-infection, as at least one isomer from Man 6 to Man 9 was significantly elevated (Figure
311 S1b & S2b). We also detected a range of sialylated structures, from mono-sialylated
312 bi-antennary to tri-sialylated tri-antennary complex-type *N*-glycans, on both cell-extracted and
313 secreted proteins. Using a PGC-LC-ESI-MS/MS workflow to enable the separation of isomers
314 based on their corresponding retention time, we found that the majority of the sialylated

315 structures displayed multiple isomeric forms (Table S1). Overall, there was an approximately
316 7% reduction in sialylated complex-type *N*-glycans in infected cells compared to their
317 mock-infected counterparts on the cell-extracted proteins. However, this overall decrease did
318 not apply uniformly to all sialylated complex-type *N*-glycan species, as some were
319 downregulated while others were either upregulated or remained unchanged in infected cells
320 (Figure S3 to S8). For example, singly sialylated bi-antennary structures with (N4H5F1S1) and
321 without core fucose (N4H5S1), along with some doubly, triply sialylated bi-antennary
322 (N4H5F1S2) and tri-antennary (N5H6S3) structures were found to be upregulated in infected
323 cells (Figure S3). On the other hand, structural isomers of the singly sialylated bi-antennary
324 structures with the composition of N4HS5F1S1, along with doubly and triply sialylated bi-
325 antennary (N4H5F1S2) and tri-antennary (N5H6F1S3) *N*-glycans were downregulated upon
326 HPIV-3 infection (Figure S4). These diverse changes in the expression of sialylated
327 complex-type *N*-glycans were detected across cell-extracted and secreted proteins, regardless
328 of post-infection time points (Figure S5-S10). Together, these findings highlight that HPIV-3
329 infection results in selective remodelling of both oligomannose and sialylated complex-type *N*-
330 glycans, with distinct changes observed at the level of individual glycan species.

331 *HPIV-3 infection modulates expression of sialic acid isomers on* N-*glycans*

332 HPIV-3 binds to sialylated glyco-epitopes on host cells via its HN protein to initiate
333 infection and later uses the same protein's neuraminidase activity to cleave sialic acids
334 (Neu5Ac), enabling the release of newly formed virions[22]. Considering this, we hypothesize
335 that HPIV-3 infection could directly affect the expressions of glycans terminating in Neu5Ac.
336 Structural isomers of sialylated complex-type *N*-glycan species arise from the linkage of
337 Neu5Ac to the terminal galactose via either an α2,3 or α2,6 glycosidic bonds on each antenna
338 of the glycan. Previous studies suggest that α2,3- and α2,6-linked Neu5Ac residues on
339 galactose serve as receptors for HPIV-3, with the viral HN neuraminidase showing a preference
340 for α2,3-linked Neu5Ac-containing glycans over their α2,6-linked counterparts[22]. Such
341 differential recognition and cleavage specificity suggest that HPIV-3 may selectively modulate
342 sialylation patterns during infection. Although sialic acid linkage isomers can be definitively
343 characterized using linkage-specific neuraminidases, the linkage of structurally simple glycans
344 bearing a single sialic acid residue can also be inferred based on their retention behaviour on
345 PGC column, as demonstrated in previously published studies[23–25]. We observed three potential
346 isomers of bi-antennary complex *N*-glycans with *m/z* 965.8^{2-} (N4H5S1). In agreement with
347 previous studies, the first two structures eluting closely on the PGC column are arm isomers of

348 an α2,6-linked mono-sialylated complex-type *N*-glycan, whereas the third structure, eluting 6
349 minutes later than the first two, represents an α2,3-linked isomer of the same composition
350 (N4H5S1)[23]. Comparing the relative abundance of these species, we found that HPIV-3
351 infection results in a significantly lower expression of the α2,3-linked isomer in both
352 cell-extracted and secreted proteins, irrespective of post-infection time points (Figure 3a & 3b).
353 On the other hand, the α2,6-linked isomer of the same *N*-glycan composition was increased in
354 infected cells when compared to the mock-infected control (Figure 3c & 3d).

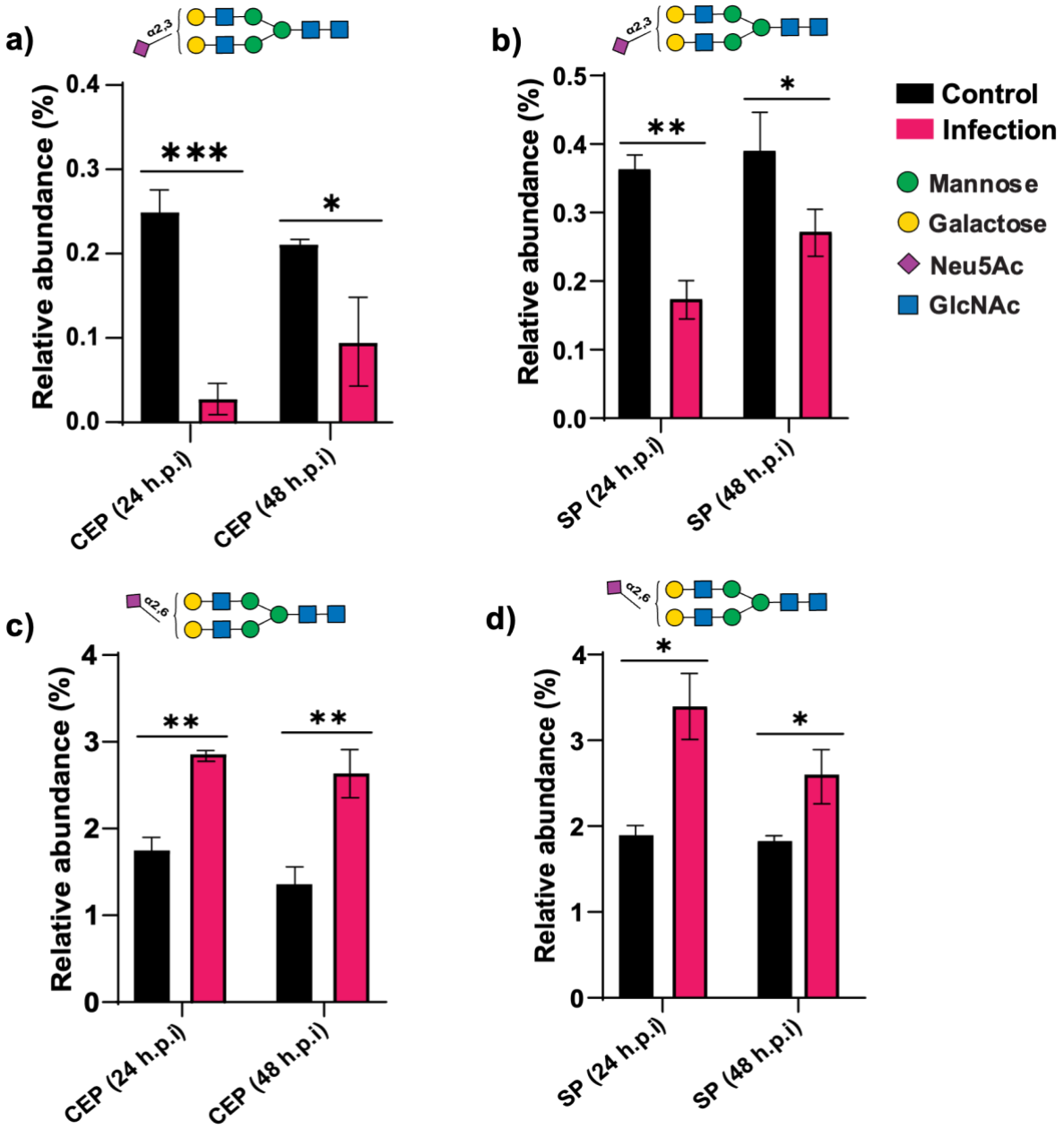

355

356 *Figure 3:* ***Differential expression of α2,3- and α2,6-linked isomers of mono-sialylated complex-type N-glycan (N4H2S1) in***
357 ***infected vs. mock-infected cells:*** *(a) α2,3 on cell-extracted proteins, (b) α2,3 on secreted proteins, (c) α2,6 on cell-extracted*
358 *proteins, (d) α2,6 on secreted proteins at 24 h and 48 h post-infection. n=3, *P<0.05, **P<0.01, ***P<0.001, unpaired*
359 *Welch's t-test. CEP: Cell extracted proteins; SP: Secreted proteins. h.p.i: hours post-infection.*

360 *Alterations in* O*-glycan profiles induced by HPIV-3 infection*

361 Since we identified significant modulation of the host-cell *N*-glycome upon HPIV-3
362 infection, we pondered if the *O*-glycome of host cell could also be altered. Like *N*-glycans,
363 *O*-glycans also have a wide range of roles in the viral replication cycle, such as facilitating viral
364 entry by acting as co-receptors and regulating viral navigation at the cell surface to assist virion
365 progeny egress[26]. Changes in the *O*-glycan profile because of HPIV-3 infection could
366 significantly affect the diverse and multifaceted functions mediated by *O*-glycans. To address
367 this open question, we investigated *O*-glycan expression at 24 h and 48 h timepoints
368 post-infection in both cell-extracted and secreted proteins. The profiling of *O*-glycans was
369 carried out essentially as described for the *N*-glycans. In total, 9 *O*-glycans structures including
370 structural isomers were detected in cell-extracted proteins from infected and mock-infected
371 A549 cells. The *O*-glycome of A549 cell is comprised of core 1 and core 2 type glycans with
372 core 2 type the most abundant (from 67% to 93% across mock-infected and infected cells). A
373 distinctive *O*-glycan profile was found on infected cell-extracted proteins when compared to
374 their mock-infected counterpart (Figure 4).

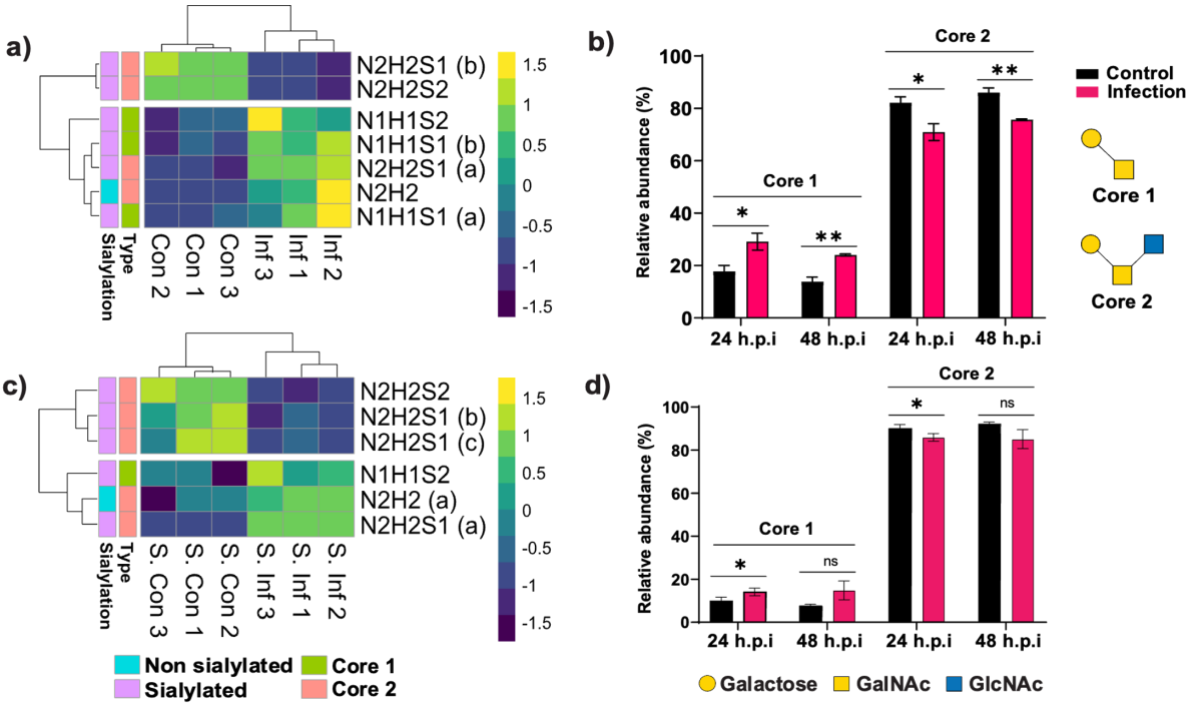

375

376 *Figure 4:* ***HPIV-3 infection modulates expression of* O*-glycans on cell-extracted and secreted proteins.*** *a) Heatmap*
377 *represents the relative abundance of significantly altered* O*-glycan species on cell-extracted proteins before and 24 h after*
378 *infection. b) Differential expression of two major core types on cell-extracted proteins at 24 h and 48 h post-infection. c)*
379 *Heatmap represents the significantly altered* O*-glycan species on secreted proteins before and 24 h post-infection. d)*
380 *Differential expression of two major core types on secreted proteins at 24 h and 48 h post-infection. n=3, *P<0.05, **P<0.01,*
381 ****P<0.001, ns: not significant, unpaired Welch's t-test. N:* N*-Acetyl Hexosamine; H: Hexose; F: Fucose; S:* N*-Acetyl*
382 *Neuraminic Acid; h.p.i: hours post-infection.*

383 We observed that core 2 type *O*-glycans from host cell-extracted proteins were downregulated
384 upon HPIV-3 infection at 24 h post-infection timepoint, reducing from 82.17% ± 2.20% in
385 mock-infected cells to 70.90% ± 3.23% in infected cells (Figure 4b). Moreover, the
386 downregulation of the core 2 type was compensated by an approximately 12% increase of
387 core 1 type in infected cells. A similar response was observed at 48 h post-infection. Next, we
388 sought to determine if the expression of *O*-glycans on secreted protein are also altered upon
389 HPIV-3 infection. A moderate decrease, from 90.10% ± 1.78% in mock-infected to
390 85.91% ± 1.78% in infected cells, of secreted protein core 2 type glycans and a corresponding
391 increase, from 9.93% ± 1.78% in mock-infected to 14.10% ± 1.77% in infected cells, of
392 secreted protein core 1 type glycans was found at 24 h timepoint post-infection (Figure 4d).
393 The same trend was found at 48 h timepoint post-infection (Figure 4d).

394 Interestingly, upon investigating individual *O*-glycan species, we observed a similar
395 pattern of infection-induced alterations across cell-extracted and secreted proteins irrespective
396 of post-infection time points. For example, the expression of the di-sialylated core 2 species on
397 cell-extracted proteins, characterized by an *m/z* of 665.2^{2-} (composed of N2H2S2), was reduced
398 by approximately three-fold, with a ~27% and 47% decrease at the 24 h and 48 h timepoints
399 post-infection, respectively in infected cells (Figure 5a and 5b). In contrast, the mono-sialylated
400 core 2 glycan [N2H2S1(a)] showed a remarkable increase in expression of ~26% and 37% at
401 24 h and 48 h timepoints post-infection, respectively upon infection (Figure 5a and 5b).

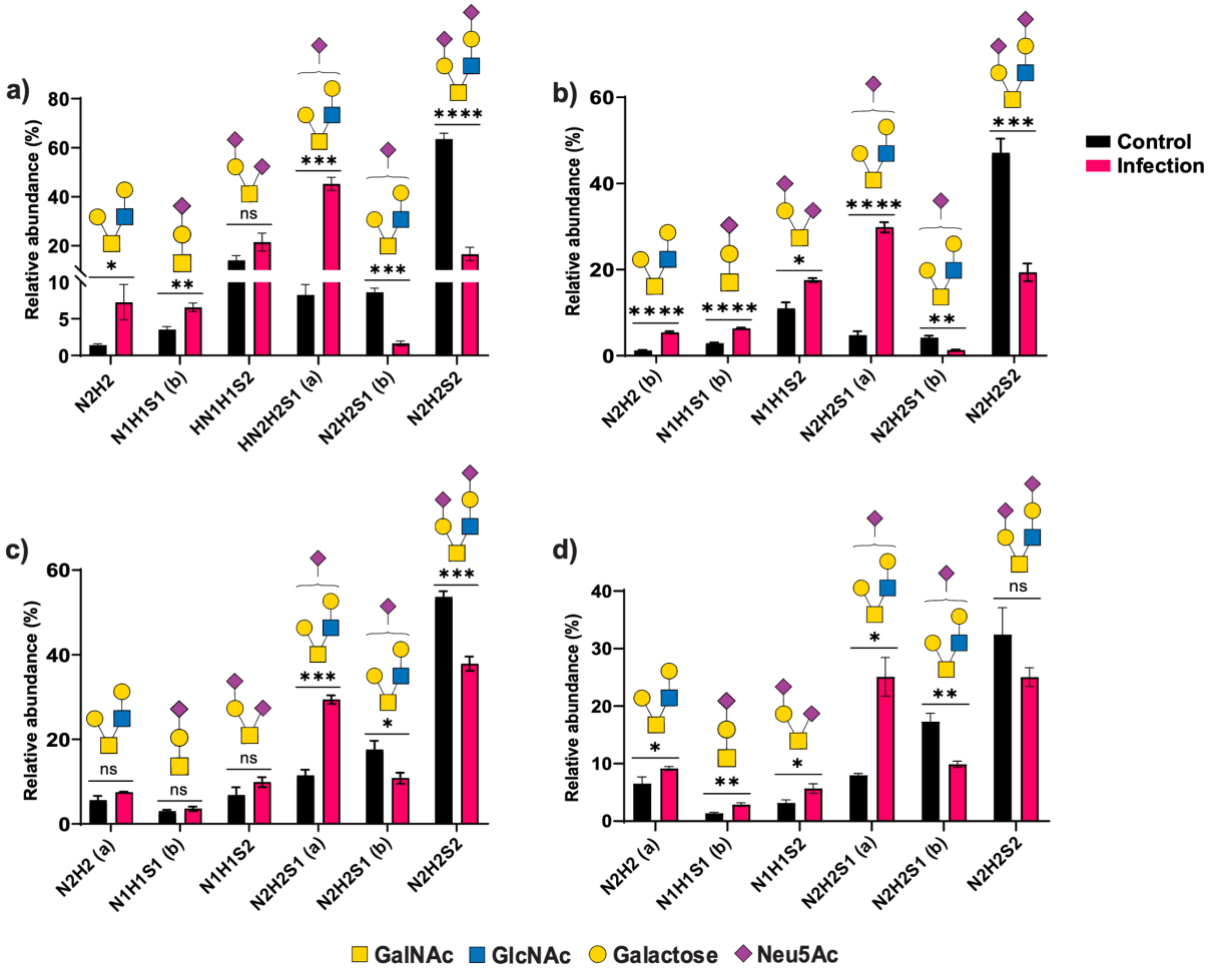

Figure 5: ***HPIV-3 triggers modulated O-glycan expression in infected and mock-infected cells.*** *Relative abundance of all the significantly altered O-glycan species on cell-extracted proteins at a) 24 h, and b) 48 h post-infection. Relative abundance of all the significantly altered O-glycan species on secreted protein at c) 24 h, and d) 48 h post-infection. n=3, *P<0.05, **P<0.01, ***P<0.001, ns: not significant, unpaired Welch's t-test. N: N-Acetyl Hexosamine; H: Hexose; S: N-Acetyl Neuraminic Acid.*

This trend was similarly observed for secreted proteins, independent of the post-infection timepoint (Figure 5c and 5d). Moreover, a structural isomer of the same composition [N2H2S1(b)] was reduced upon infection across cell-extracted and secreted proteins (Figure 5a-d). Interestingly, a core 1 type doubly-sialylated *O*-glycan, with a composition of N1H1S2, was found to be significantly elevated in infected cells for both cell-extracted and secreted proteins at each post-infection timepoint (Figure 5a-d). We observed a slightly favourable expression of core 1 type *O*-glycans compared to core 2 type, along with altered expression of glycans carrying specific sialylated glyco-motifs in response to infection. These changes were consistent for glycans released from both cell-extracted and secreted proteins, regardless of post-infection time points.

419 *HPIV-3 infection induces remodelling of glycosphingolipid (GSL)-associated glycans*

420 GSL glycans represent a significant portion of the host glycome and are primarily
421 located on the cellular plasma membrane, where their sugar moieties are exposed to the external
422 environment[14]. These glycans are involved in various biological processes, including
423 infections[27]. Some viruses (e.g HPIV-3[22], HIV[28], Polyomavirus[29]) are historically known to
424 utilize GSL glycans in their life cycle. However, no studies have reported host cell GSL glycan
425 dynamics in response to parainfluenza viral infection. To characterize GSL glycans, GSLs were
426 extracted from both infected and mock-infected cells before the enzymatic release of the
427 glycans from the head groups, which were then analysed by PGC-LC-ESI-MS/MS. In total, 12
428 GSL glycan species were detected, and the relative intensities of each glycan species were
429 compared between infected and mock-infected control. The structure of some of the GSL
430 glycans could only be partially resolved in this study due to the absence of informative
431 fragment ions in tandem MS, and the lack of *exo*-glycosidase digestion in our study. Therefore,
432 there were no GSL glycans class wide comparison made between infected and mock-infected
433 controls. However, major alterations have been detected at the individual glycan level in
434 infected cells (Figure 6).

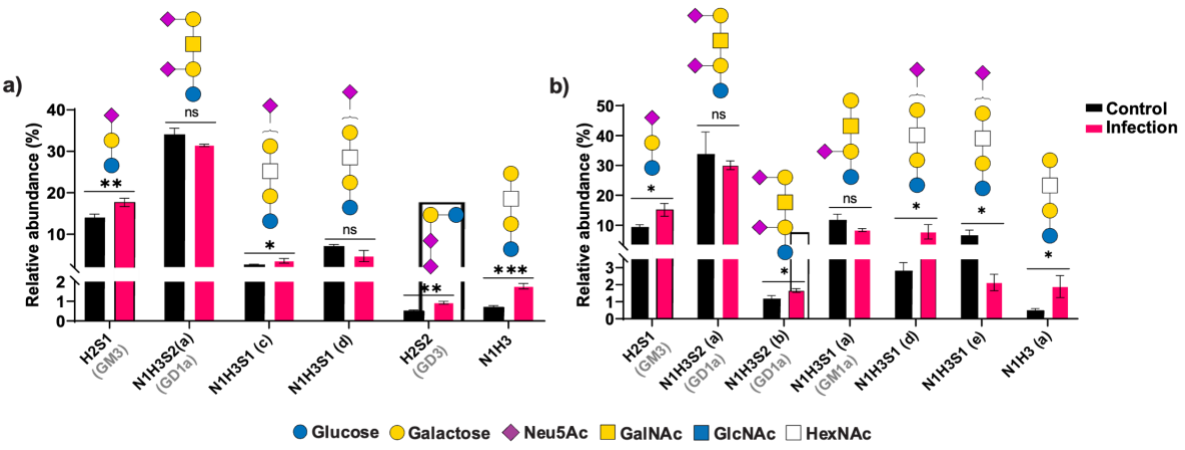

435

436 *Figure 6:* ***HPIV-3 infection triggers altered expression of GSL glycans.*** *Relative expression of all the significantly altered*
437 *GSL glycan species at a) 24 h, and b) 48 h post-infection. n=3, *P<0.05, **P<0.01, ***P<0.001, ns: not significant, unpaired*
438 *Welch's t-test. N: N-Acetyl Hexosamine; H: Hexose; S: N-Acetyl Neuraminic Acid.*

439 Gangliosides containing one and two Neu5Ac residues were the most abundant GSL glycan
440 types in A549 cells followed by the neo(lacto)-series. The GSL glycan, comprised of H2S1
441 (GM3), appeared to be increased in expression from 14.0% ± 0.84% in mock-infected cells to
442 17.66% ± 1.01% in infected cells, 24 h post-infection (Figure 6a). The increased expression of
443 GM3 remained stable even at 48 h timepoint post-infection (Figure 6b). Another ganglioside

444 comprised of N1H3S2 (GD1a), the most abundant GSL glycan in A549 cells, was reduced in
445 expression from 34.02% ± 1.57% in mock-infected cells to 31.44% ± 0.27% in infected cells,
446 at 24 h timepoint post-infection. A similar trend was observed at 48 h timepoint post-infection
447 despite the change not being statistically significant. Additionally, several other GSL glycan
448 species were also observed to be altered in response to HPIV-3 infection. Two partially resolved
449 isomers with the composition of H3N1S1 (presumably sialylated neo(lacto)-series or GM1
450 gangliosides) showed an opposite trend to each other upon infection. The changes were more
451 prominent at 48 h timepoint post-infection when compared to the mock-infected control.
452 Interestingly, a previous study reported that the sialylated neo(lacto)-series, with the same
453 composition, is recognised by HPIV-3 using a solid-phase binding assay[22]. Higher expression
454 of one of the H3N1S1 isomers in infected cells could be attributed to the reduced expression
455 of GD1 (H3N1S2), as HPIV-3 HN mediated sialic acid cleavage from GD1 glycan would
456 potentially generate a glycan with the composition of H3N1S1, thereby contributing to overall
457 increase of that species upon infection. Furthermore, the expression of GD3 (H2S2) was found
458 to be elevated only at 24 h timepoint post-infection and no significant change was observed at
459 48 h timepoint post-infection. A precursor glycan, belonging to either gangliosides or
460 neo(lacto)-series, with composition of H3N1 was found to be elevated at both 24 h and 48 h
461 timepoints post-infection.

462 **Discussion**

463 Every cell in nature is decorated with a dense layer of carbohydrates (glycans)
464 covalently linked to proteins or lipids, forming the glycocalyx. These glycans form the
465 foundation of a universal biological language known as the glycome, playing active roles in
466 numerous cellular processes[21]. However, microorganisms such as viruses exploit these cell
467 surface resident glycans by using them as receptors or co-receptors. Additionally, viruses take
468 advantage of the host-cell glyco-machinery to decorate their own surface proteins with glycans,
469 acting as protective shields to evade the host immune response[25,26]. During human evolution,
470 viruses along with other pathogens such as bacteria and parasites have co-evolved with their
471 human host and consequently have actively participated in the remodelling of the human cell
472 glycome[32]. For instance, it is widely accepted that evolutionary pressure from pathogens played
473 a significant role in the loss of certain carbohydrates, such as *N*-glycolylneuraminic acid
474 (Neu5Gc) and α-Gal, in human[33,34].

475 To date, only a few studies have described the changes in host-cell glycosylation upon
476 viral infection and the role of an altered glycome expression in triggering innate immune
477 response[6,35,36]. For example, a lectin microarray based study has suggested a significant
478 increase of oligomannose-type glycans in ferret lung upon influenza virus infection, which was
479 further found to be associated with disease severity[6]. More recently, several studies on
480 SARS-CoV-2 infection observed an altered glycosylation profile on antibodies against the viral
481 spike protein with lower fucosylation and sialylation, that ultimately affects the effector
482 functions of antibodies[35,36]. However, these studies either did not employ more sensitive
483 techniques like mass spectrometry or focused solely on the glycosylation of antibody (IgG)
484 against viral protein, rather than examining the glycosylation of infected host-cells. To the best
485 of our knowledge, there is no reported study on the host-cell glycome response to HPIV-3
486 infection. Thus, we employed a highly sensitive mass spectrometry technique coupled with
487 porous graphitized carbon liquid chromatography to reveal the global glycosylation (*N*-, *O*- and
488 GSL glycans) changes of HPIV-3-infected cells. Our analysis revealed an approximately 5%
489 to 12% increase of oligomannose-type *N*-glycans on cell-extracted and secreted proteins, both
490 at 24 h and 48 h post-infection timepoints. This increase may reflect a host cellular response to
491 infection-induced activation of the unfolded protein response (UPR), as has been proposed in
492 other viral systems, such as influenza infection in the ferret lung[6]. The UPR is a
493 well-characterized cellular stress mechanism that is activated when unfolded or misfolded
494 proteins accumulate in the endoplasmic reticulum (ER), disrupting protein homeostasis[37]. In
495 response, the cell initiates UPR signalling to restore ER function by enhancing the folding
496 capacity of the ER, reducing protein translation, and promoting the degradation of misfolded
497 proteins[37]. One important hallmark of UPR activation is the increase in oligomannose-type
498 *N*-glycans, which are essential intermediates in the early stages of protein glycosylation and
499 folding[6,38]. These glycans are particularly important for the quality control of nascent
500 glycoproteins, as they interact with ER-resident chaperones such as calnexin and calreticulin[38].
501 This interaction ensures that only properly folded proteins proceed along the secretory pathway,
502 while misfolded proteins are retained and targeted for ER-associated degradation (ERAD)[32].
503 In the context of HPIV-3 infection, we observe an increase in oligomannose-type glycans which
504 may reflect a host-cellular response to the stress placed on the ER to fold both viral and cellular
505 proteins. Viral infection frequently disrupts ER homeostasis, not only due to synthesis of viral
506 proteins but also through inflammation-induced oxidative stress and altered calcium
507 signalling[39,40]. As a result, the host cell may ramp up UPR signalling to maintain protein
508 homeostasis—not only for its own proteins, such as membrane receptors, transporters, or

509 immune-modulatory proteins, which are critical for cellular survival and antiviral responses—
510 but also for the proper folding and processing of viral proteins[41,42]. Together, our findings
511 support the hypothesis that the increased abundance of oligomannose-type *N*-glycans is driven
512 by UPR-mediated adaptation aimed at preserving ER function and protein quality control
513 during HPIV-3 infection. However, direct evidence for UPR activation in our system is still
514 lacking. Future studies employing transcriptomics or proteomics analysis, particularly
515 monitoring UPR markers such as BiP/GRP78, CHOP, and XBP1 splicing, will be essential to
516 confirm whether the UPR pathway is indeed engaged in HPIV-3-infected cells and driving the
517 observed glycomic changes[6]. Furthermore, the increased expression of oligomannose-type
518 *N*-glycan was accompanied by overall reduction of sialylated complex-type glycans on
519 cell-extracted and secreted proteins, irrespective of post-infection time points. We hypothesize
520 that the elevated expression of oligomannose-type *N*-glycans contributes to the downregulation
521 of sialylated complex-type *N*-glycans through two potential mechanisms. First, the
522 accumulation of oligomannose structures may saturate the glycosylation machinery within the
523 Golgi apparatus, thereby limiting the processing capacity for downstream glycan maturation.
524 Second, as the biosynthesis of complex-type *N*-glycans requires the prior trimming of
525 oligomannose precursors, excessive levels of these unprocessed glycans may reduce the
526 availability of appropriately processed substrates necessary for complex glycan formation[5].
527 Future studies incorporating transcriptomic and proteomic analysis will benefit from evaluating
528 the expression levels of Golgi-resident mannosidases and glycosyltransferases to confirm
529 whether elevated oligomannose levels contribute to the reduction in complex-type *N*-glycan
530 expression[6,43]. These studies, together with the existing glycomic data, may determine whether
531 the reduction in complex-type *N*-glycan expression upon HPIV-3 infection is caused by limited
532 substrate availability, as complex glycan synthesis requires the prior trimming of
533 oligomannose, or by saturation of the glycosylation machinery due to an overload of
534 oligomannose substrates.

535 Moreover, we were able to identify α2,3- and α2,6-linked isomers with the composition
536 of N4H5S1, based on chromatographic separation, together with MS fragmentation[23].
537 Interestingly, HPIV-3 infection leads to a lower expression of *N*-glycans containing α2,3-linked
538 sialic acid and an increase of its α2,6-linked counterpart, with the same composition (N4H5S1).
539 A previous study found that HPIV-3 utilizes α2,3- and α2,6-linked *N*-acetylneuraminic acid
540 (Neu5Ac) to galactose as receptors, with a higher HPIV-3 HN neuraminidase activity observed
541 for α2,3-linked Neu5Ac[22]. Thus, the downregulation of α2,3-linked sialylated isomeric

542 glycans, in this instance, could be attributed to the HPIV-3 HN neuraminidase activity,
543 mediating the cleavage of receptor glycans at the end of each viral replication cycle[44].
544 Furthermore, we hypothesize that higher expression of α2,6-linked isomer of N4H5S1 in
545 infected cells could be a consequence of the α2,3-linked sialic acid trimming of N4H5S2
546 (Figure S4, S6, S8, S10), as the HPIV-3 HN-mediated cleavage of N4H5S2 glycan would
547 potentially generate glycan with the composition of HN4H5N1. To confirm the intrinsic role
548 of HN protein on the reduction of sialylated *N*-glycans it would be interesting to treat infected
549 cells with a specific inhibitor to HN protein[45]. Moreover, as glycan biosynthesis is a sequential
550 enzymatic process, the modulation of sialylated complex-type *N*-glycans expression could also
551 be the result of virus infection-mediated changes in enzyme expression related to glycan
552 biosynthesis[21]. A bulk RNA-seq analysis of infected and mock-infected cells might enable us
553 to identify the expression profiles of enzymes involved in glycan biosynthesis, thereby
554 uncovering potential mechanisms underlying the observed changes in *N*-glycans upon
555 infection.

556 The impact of HPIV-3 infection in the host-cell *O*-glycome is significant and we have
557 observed that there is a significant reduction of core 2 type as well as a higher expression of
558 core 1 type *O*-glycans across host cell-extracted and secreted proteins. A recent study also
559 described an approximately 2.5-fold downregulation of core 2 *N*-acetylglucosamine transferase
560 (GlcNAcT) enzyme upon HPIV-3 infection on A549 cells[43]. We propose that the reduction of
561 core 2 type *O*-glycans could be the result of downregulation of the core 2
562 β1,6-*N*-acetylglucosaminyltransferase (Core 2 GlcNAc-T) enzyme that acts on core 1 type to
563 make core 2 type *O*-glycans. Furthermore, concomitant with the observed down regulation of
564 core 2 type *O*-glycans upon HPIV-3 infection, we also detected a down-regulation of doubly
565 sialylated core 2 type glycans with a corresponding higher expression of singly sialylated
566 core 2 type structures in infected cells. Similar for the downregulation of α2,3-linked sialylated
567 isomeric *N*-glycans, we infer that the reduction of doubly sialylated core 2 type structures is
568 caused by the neuraminidase activity of the HPIV-3 HN protein which subsequently results in
569 the upregulation of similar glycans with one less Neu5Ac[46]. Again, to verify the specific role
570 of the HPIV-3 HN protein in the reduction of doubly-sialylated *O*-glycans, it would be valuable
571 to treat infected cells with a specific inhibitor of the HN protein[45] and determine the expression
572 of doubly-sialylated *O*-glycans. Nonetheless, these changes may have profound implications
573 for host-cell glycosylation profiles, influencing immune responses and potentially contributing
574 to the pathogenesis of the virus[6,43].

575 GSL glycans significantly contribute to the formation of cellular glycome and some
576 viruses including HPIV-3 are known to exploit GSL glycans in their life cycle[22]. In our analysis,
577 gangliosides account for approximately 60% of the total GSL glycan population in A549 cells,
578 underscoring their dominance in the glycan landscape of the respiratory epithelium. HPIV-3
579 triggers altered expression of gangliosides glycans including GM1, GM3, and GD3, which are
580 often implicated in viral replication cycle[27]. These gangliosides have been previously
581 implicated in modulating viral replication, either by serving as entry cofactors or by influencing
582 intracellular signalling pathways essential for viral propagation[47,48]. For example, GM1 serves
583 as entry receptors for simian virus 40 (SV40)[49], while GM3 plays a dual role in cell
584 physiology[50] and viral pathogenesis, including facilitating influenza virus infection by
585 modulating membrane dynamics and virus-host interactions[51]. Furthermore, GM3 has been
586 shown to regulate cell proliferation and differentiation by modulating receptor tyrosine kinases
587 such as epidermal growth factor receptor (EGFR)[52]. During viral infection, these signalling
588 pathways are often hijacked to support viral replication and suppress host antiviral
589 responses[53,54]. GD3 ganglioside is also implicated in viral infection, particularly those affecting
590 nervous system[55]. Altogether, changes in ganglioside expression during HPIV-3 infection
591 might represent either a viral adaptation to enhance conditions for its replication, or a host-cell
592 mechanism to manage the infection.

593 The second most common type of GSL glycans detected in A549 cells was the
594 neo(lacto)-series. A previous study reported a sialylated neo(lacto)-series glycan as a potential
595 receptor for HPIV-3[22]. In our study we found a potential sialylated neo(lacto)-series glycan was
596 downregulated upon HPIV-3 infection. We hypothesize that the cleavage of sialic acid,
597 mediated by HPIV-3 HN, may contribute to the reduction of sialylated neo(lacto)-series
598 glycans on HPIV-3 infected cells. Furthermore, few other glycans, which were not recognised
599 as binding factors, have also been found to be altered after HPIV-3 infection in our study. We
600 hypothesize a similar receptor specificity analysis using altered GSL glycans (GM1, GM3,
601 GD3) could potentially identify few other GSL glycans as binding factors.

602 Conclusion

603 Using advanced mass spectrometry-based glycomics, we investigated HPIV-3–induced
604 alterations in the glycome of A549 human lung epithelial cells. Our analysis revealed
605 approximately 116 distinct glycan species in both HPIV-3–infected and mock-infected cells,
606 highlighting the complexity and diversity of the host-cell glycome. Importantly, this study

607 provides the first experimental evidence that HPIV-3 infection induces marked alterations in
608 the host cell glycome—spanning all three major glycan types (*N*-, *O*-, and glycosphingolipid
609 glycans). These alterations suggest that HPIV-3 infection significantly remodels the host cell
610 surface and secretory glycan landscape, potentially influencing key biological processes such
611 as virus-host interactions, immune recognition, and intracellular signalling. Furthermore, our
612 analytical approach provides a valuable platform for characterizing virus-induced glycomic
613 changes and can be readily adapted to study other respiratory viruses, e.g., influenza virus,
614 thereby paving the way for a better understanding of the roles of glycans in viral pathogenesis.

615 Acknowledgement

616 This research was partially funded by Griffith University International Postgraduate
617 Research Scholarship (GUIPRS) and Griffith University Postgraduate Research Scholarship
618 (GUPRS) (P.K.D). We gratefully acknowledge funding from the National Health and Medical
619 Research Council (NHMRC) (MvI., APP1047824 & GNT1196520) and a Peter Doherty
620 Biomedical Early Career Fellowship (L.D., GNT1157150). We thank Dr. Thomas Litfin and
621 Anuk Indraratna for assisting in data visualization.

622 Author contributions

623 Conceptualisation: P.K.D., L.D., B.B., P.G., A.E.D, M.v.I.; methodology: P.K.D., P.G.,
624 A.E.D.; investigation: P.K.D.; analysis: P.K.D.; writing—original draft: P.K.D.; writing—
625 review and editing: L.D., P.G., B.B., A.E.D., M.v.I.; funding acquisition: L.D., M.v.I.

626 Abbreviations,

627 HPIV: Human parainfluenza virus
628 HN: haemagglutinin-neuraminidase
629 H.p.i: Hour's post-infection
630 CEP: Cell extracted protein
631 SP: Secreted protein
632 HN: *N*-Acetyl Glucosamine
633 H: Hexose
634 dH: Deoxyhexose
635 Man: Mannose
636 N: *N*-Acetyl Neuraminic Acid

637 G: *N*-glycolylneuraminic Acid
638 GSL: Glycosphingolipids
639 PGC: Porous graphitized carbon
640 ESI: Electrospray ionization
641 CID: Collision induced dissociation.
642

Reference

643 1. Branche, A. R. & Falsey, A. R. Parainfluenza Virus Infection. *Semin. Respir. Crit.*
644 *Care Med.* **37**, 538–554 (2016).

645 2. Castleman, W. L., Northrop, P. J. & McAllister, P. K. Replication of parainfluenza
646 type-3 virus and bovine respiratory syncytial virus in isolated bovine type-II
647 alveolar epithelial cells. *Am. J. Vet. Res.* **52**, 880–885 (1991).

648 3. Wl, C., Pj, N. & Pk, M. Replication of parainfluenza type-3 virus and bovine
649 respiratory syncytial virus in isolated bovine type-II alveolar epithelial cells. *Am.*
650 *J. Vet. Res.* **52**, (1991).

651 4. Saha, S., Grimwood, K., Lambert, S. B., Sarna, M. & Ware, R. S. Parainfluenza
652 Virus Infection in an Australian Community-based Birth Cohort. *Pediatr. Infect.*
653 *Dis. J.* **39**, e284 (2020).

654 5. Reily, C., Stewart, T. J., Renfrow, M. B. & Novak, J. Glycosylation in health and
655 disease. *Nat. Rev. Nephrol.* **15**, 346–366 (2019).

656 6. Heindel, D. W. *et al.* Glycomic analysis of host response reveals high mannose as
657 a key mediator of influenza severity. *Proc. Natl. Acad. Sci. U. S. A.* **117**, 26926–
658 26935 (2020).

659 7. Quiñones-Kochs, M. I., Buonocore, L. & Rose, J. K. Role of N-Linked Glycans
660 in a Human Immunodeficiency Virus Envelope Glycoprotein: Effects on Protein
661 Function and the Neutralizing Antibody Response. *J. Virol.* **76**, 4199–4211 (2002).

662 8. Watanabe, Y., Bowden, T. A., Wilson, I. A. & Crispin, M. Exploitation of
663 glycosylation in enveloped virus pathobiology. *Biochim. Biophys. Acta Gen. Subj.*
664 **1863**, 1480–1497 (2019).

665 9. Dirr, L. *et al.* The catalytic mechanism of human parainfluenza virus type 3
666 haemagglutinin-neuraminidase revealed. *Angew. Chem. Int. Ed Engl.* **54**, 2936–
667 2940 (2015).

668 10. Tabang, D. N., Ford, M. & Li, L. Recent Advances in Mass Spectrometry-Based
669 Glycomic and Glycoproteomic Studies of Pancreatic Diseases. *Front. Chem.* **9**,
670 (2021).

671 11. Ashwood, C., Lin, C.-H., Thaysen-Andersen, M. & Packer, N. H. Discrimination
672 of Isomers of Released N- and O-Glycans Using Diagnostic Product Ions in
673 Negative Ion PGC-LC-ESI-MS/MS. *J. Am. Soc. Mass Spectrom.* **29**, 1194–1209
674 (2018).

675 12. Zhang, T. *et al.* Differential O- and Glycosphingolipid Glycosylation in Human
676 Pancreatic Adenocarcinoma Cells With Opposite Morphology and Metastatic
677 Behavior. *Front. Oncol.* **10**, 732 (2020).

678 13. Jensen, P. H., Karlsson, N. G., Kolarich, D. & Packer, N. H. Structural analysis of
679 N- and O-glycans released from glycoproteins. *Nat. Protoc.* **7**, 1299–1310 (2012).

680 14. Wang, D. *et al.* Glycosphingolipid-Glycan Signatures of Acute Myeloid Leukemia
681 Cell Lines Reflect Hematopoietic Differentiation. *J. Proteome Res.* **21**, 1029–
682 1040 (2022).

683 15. MacLean, B. *et al.* Skyline: an open source document editor for creating and
684 analyzing targeted proteomics experiments. *Bioinformatics* **26**, 966–968 (2010).

685 16. Cooper, C. A., Gasteiger, E. & Packer, N. H. GlycoMod--a software tool for
686 determining glycosylation compositions from mass spectrometric data.
687 *Proteomics* **1**, 340–349 (2001).

688 17. Ceroni, A. *et al.* GlycoWorkbench: A Tool for the Computer-Assisted Annotation
689 of Mass Spectra of Glycans. *J. Proteome Res.* **7**, 1650–1659 (2008).

690 18. Campbell, M. P. & Packer, N. H. UniCarbKB: New database features for
691 integrating glycan structure abundance, compositional glycoproteomics data, and
692 disease associations. *Biochim. Biophys. Acta* **1860**, 1669–1675 (2016).

693 19. Everest-Dass, A. V., Abrahams, J. L., Kolarich, D., Packer, N. H. & Campbell, M.
694 P. Structural Feature Ions for Distinguishing ***N-*** and ***O-*** Linked Glycan Isomers
695 by LC-ESI-IT MS/MS. *J. Am. Soc. Mass Spectrom.* **24**, 895–906 (2013).

696 20. Crouch, L. I. *et al.* The role of glycans in health and disease: Regulators of the
697 interaction between gut microbiota and host immune system. *Semin. Immunol.* **73**,
698 101891 (2024).

699 21. Schjoldager, K. T., Narimatsu, Y., Joshi, H. J. & Clausen, H. Global view of human
700 protein glycosylation pathways and functions. *Nat. Rev. Mol. Cell Biol.* **21**, 729–
701 749 (2020).

702 22. T, S. *et al.* Receptor specificities of human respiroviruses. *J. Virol.* **75**, (2001).

703 23. M, A. *et al.* Specific glycosylation of membrane proteins in epithelial ovarian
704 cancer cell lines: glycan structures reflect gene expression and DNA methylation
705 status. *Mol. Cell. Proteomics MCP* **13**, (2014).

706 24. Young, C. *et al.* In-House Packed Porous Graphitic Carbon Columns for Liquid
707 Chromatography-Mass Spectrometry Analysis of N-Glycans. *Front. Chem.* **9**,
708 653959 (2021).

709 25. Jl, A., Mp, C. & Nh, P. Building a PGC-LC-MS N-glycan retention library and
710 elution mapping resource. *Glycoconj. J.* **35**, (2018).

711 26. Olofsson, S., Bally, M., Trybala, E. & Bergström, T. Structure and Role of O-
712 Linked Glycans in Viral Envelope Proteins. *Annu. Rev. Virol.* **10**, 283–304 (2023).

713 27. Aerts, J. M. F. G., Artola, M., van Eijk, M., Ferraz, M. J. & Boot, R. G.
714 Glycosphingolipids and Infection. Potential New Therapeutic Avenues. *Front.*
715 *Cell Dev. Biol.* **7**, 324 (2019).

716 28. Lingwood, C. A. & Branch, D. R. The role of glycosphingolipids in HIV/AIDS.
717 *Discov. Med.* **11**, 303–313 (2011).

718 29. Taube, S., Jiang, M. & Wobus, C. E. Glycosphingolipids as Receptors for Non-
719 Enveloped Viruses. *Viruses* **2**, 1011–1049 (2010).

720 30. Bagdonaite, I. & Wandall, H. H. Global aspects of viral glycosylation.
721 *Glycobiology* **28**, 443–467 (2018).

722 31. Feng, T. *et al.* Glycosylation of viral proteins: Implication in virus–host interaction
723 and virulence. *Virulence* **13**, 670–683 (2022).

724 32. Markine-Goriaynoff, N. *et al.* Glycosyltransferases encoded by viruses. *J. Gen.*
725 *Virol.* **85**, 2741–2754 (2004).

726 33. Singh, S. *et al.* Loss of α-gal during primate evolution enhanced antibody-effector
727 function and resistance to bacterial sepsis. *Cell Host Microbe* **29**, 347-361.e12
728 (2021).

729 34. Altman, M. O. & Gagneux, P. Absence of Neu5Gc and Presence of Anti-Neu5Gc
730 Antibodies in Humans—An Evolutionary Perspective. *Front. Immunol.* **10**, 789
731 (2019).

732 35. Larsen, M. D. *et al.* Afucosylated IgG characterizes enveloped viral responses and
733 correlates with COVID-19 severity. *Science* **371**, eabc8378 (2021).

734 36. Chakraborty, S. *et al.* Proinflammatory IgG Fc structures in patients with severe
735 COVID-19. *Nat. Immunol.* **22**, 67–73 (2021).

736 37. Read, A. & Schröder, M. The Unfolded Protein Response: An Overview. *Biology*
737 **10**, 384 (2021).

738 38. Wong, M. Y. *et al.* XBP1s activation can globally remodel N-glycan structure
739 distribution patterns. *Proc. Natl. Acad. Sci.* **115**, E10089–E10098 (2018).

740 39. Victor, P., Sarada, D. & Ramkumar, K. M. Crosstalk between endoplasmic
741 reticulum stress and oxidative stress: Focus on protein disulfide isomerase and
742 endoplasmic reticulum oxidase 1. *Eur. J. Pharmacol.* **892**, 173749 (2021).

743 40. Carreras-Sureda, A., Pihán, P. & Hetz, C. Calcium signaling at the endoplasmic
744 reticulum: fine-tuning stress responses. *Cell Calcium* **70**, 24–31 (2018).

745 41. Slaine, P. D. *et al.* Thiopurines Activate an Antiviral Unfolded Protein Response
746 That Blocks Influenza A Virus Glycoprotein Accumulation. *J. Virol.* **95**,
747 10.1128/jvi.00453-21 (2021).

748 42. Rufo, N., Garg, A. D. & Agostinis, P. The Unfolded Protein Response in
749 Immunogenic Cell Death and Cancer Immunotherapy. *Trends Cancer* **3**, 643–658
750 (2017).

751 43. Blanco-Melo, D. *et al.* Imbalanced Host Response to SARS-CoV-2 Drives
752 Development of COVID-19. *Cell* **181**, 1036-1045.e9 (2020).

753 44. Amonsen, M., Smith, D. F., Cummings, R. D. & Air, G. M. Human Parainfluenza
754 Viruses hPIV1 and hPIV3 Bind Oligosaccharides with α2-3-Linked Sialic Acids
755 That Are Distinct from Those Bound by H5 Avian Influenza Virus Hemagglutinin.
756 *J. Virol.* **81**, 8341–8345 (2007).

757 45. Guillon, P. *et al.* Structure-guided discovery of potent and dual-acting human
758 parainfluenza virus haemagglutinin-neuraminidase inhibitors. *Nat. Commun.* **5**,
759 5268 (2014).

760 46. Amonsen, M., Smith, D. F., Cummings, R. D. & Air, G. M. Human Parainfluenza
761 Viruses hPIV1 and hPIV3 Bind Oligosaccharides with α2-3-Linked Sialic Acids
762 That Are Distinct from Those Bound by H5 Avian Influenza Virus Hemagglutinin.
763 *J. Virol.* **81**, 8341 (2007).

764 47. Das, A. *et al.* Gangliosides are essential endosomal receptors for quasi-enveloped
765 and naked hepatitis A virus. *Nat. Microbiol.* **5**, 1069–1078 (2020).

766 48. Mazzon, M. & Mercer, J. Lipid interactions during virus entry and infection. *Cell.*
767 *Microbiol.* **16**, 1493–1502 (2014).

768 49. Tsai, B. *et al.* Gangliosides are receptors for murine polyoma virus and SV40.
769 *EMBO J.* **22**, 4346–4355 (2003).

770 50. Nojiri, H., Takaku, F., Terui, Y., Miura, Y. & Saito, M. Ganglioside GM3: an acidic
771 membrane component that increases during macrophage-like cell differentiation
772 can induce monocytic differentiation of human myeloid and monocytoid leukemic
773 cell lines HL-60 and U937. *Proc. Natl. Acad. Sci.* **83**, 782–786 (1986).

774 51. Vrijens, P. *et al.* Influenza virus entry via the GM3 ganglioside-mediated platelet-
775 derived growth factor receptor β signalling pathway. *J. Gen. Virol.* **100**, 583–601
776 (2019).

777 52. Coskun, Ü., Grzybek, M., Drechsel, D. & Simons, K. Regulation of human EGF
778 receptor by lipids. *Proc. Natl. Acad. Sci. U. S. A.* **108**, 9044–9048 (2011).

779 53. Ryu, J.-S. *et al.* Ganglioside GM3 Up-Regulate Chondrogenic Differentiation by
780 Transform Growth Factor Receptors. *Int. J. Mol. Sci.* **21**, 1967 (2020).

781 54. Fan, Y., Sanyal, S. & Bruzzone, R. Breaking Bad: How Viruses Subvert the Cell
782 Cycle. *Front. Cell. Infect. Microbiol.* **8**, 396 (2018).

783 55. Cutillo, G., Saariaho, A.-H. & Meri, S. Physiology of gangliosides and the role of
784 antiganglioside antibodies in human diseases. *Cell. Mol. Immunol.* **17**, 313–322
785 (2020).